ISSN 0023-1584, Kinetics and Catalysis, 2021, Vol. 62, No. 3, pp. 418–427. © Pleiades Publishing, Ltd., 2021.
Russian Text © The Author(s), 2021, published in Kinetika i Kataliz, 2021, Vol. 62, No. 3, pp. 368–378.

Methanol to Aromatic Reaction over HZSM-5: Co-Effect Desilication and SiO_2 Deposition

Hui Li[a], Peng Dong[a], Dong Ji[a], Xinhong Zhao[a], Chunqiang Li[a], and Guixian Li[a, *]

[a] *College of Petrochemical Technology, Lanzhou University of Technology, Lanzhou, 730050 China*

**e-mail: lgxwyf@163.com*

Received July 27, 2020; revised December 18, 2020; accepted December 23, 2020

Abstract—In this work Si/HZSM-5-0.09M catalyst was prepared using desilication and regrowth of SiO_2 method, which was characterized by XRF, XRD, SEM, NH_3-TPD, and N_2 adsorption/desorption. Meanwhile, the structure–activity relationship was comprehensively discussed. The results revealed that the aromatics total selectivity of Si/HZSM-5-0.09M catalyst was significantly improved, from 33 to 54.8% compared to HZSM-5 under the optimal conditions. Also, the selectivity of *p*-xylene over Si/HZSM-5-0.09M catalyst increased from 4.6 to 19.8% compared to HZSM-5. The total selectivity of benzene, toluene, and xylene over Si/HZSM-5-0.09M catalyst was significantly improved by 66.1% compared to that of HZSM-5. Thus, an excellent catalytic effect has been found, which indicates that the SiO_2 deposition on the surface favors the enhancement of the *p*-xylene selectivity in the methanol aromatization reaction.

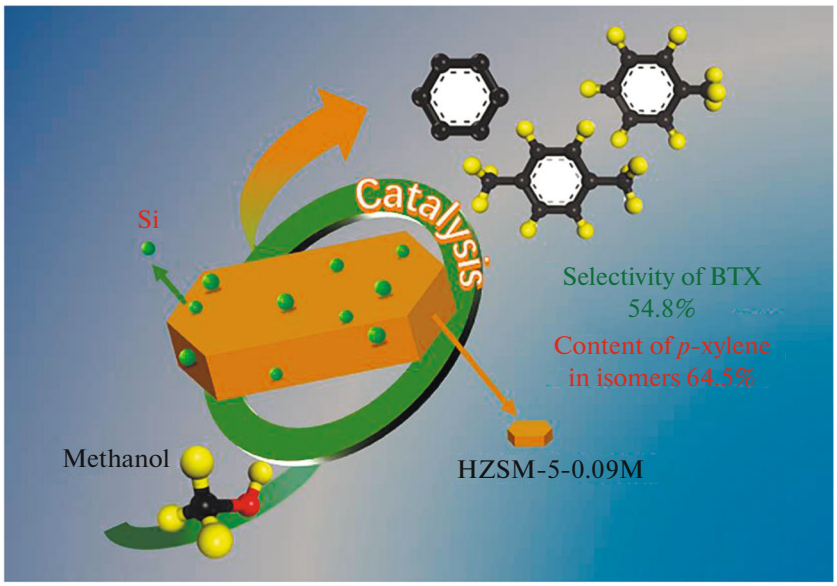

Keywords: HZSM-5, methanol, *p*-xylene, selectivity, MTA reaction

DOI: 10.1134/S0023158421030058

INTRODUCTION

Reports indicate that light aromatics, key materials in petrochemical, perfumery, dyestull, and polymer industry could be produced from the resource of crude oil by alkylation, naphtha reforming, or oil thermal cracking [1]. Notably, the production of BTX, specifically *p*-xylene, does not presently meet the market demand due to the shortages in fossil oil and fluctuating prices [2–4]. However, with the development of the C_1 chemical, the above challenges have been effectively mitigated by a series of methanol reactions, since methanol could be easily and largely obtained via syngas ($CO/CO_2 + H_2$), from coal, natural gas, coal bed gas, and biomass [5, 6]. So far, methanol to gasoline

Abbreviarions: BTX, benzene-toluent-xylene; MTG, methanol to gasoline; MTO, methanol to olefins; MTP, methanol to propylene; MTA, methanol to aromatic; MTH, methanol to hydrocarbon; TEOS, tetraethoxysilane; XRD, X-ray diffraction; SEM, scanning electron microscopy; XRF, X-ray fluorescence analysis; NH_3-TPD, temperature-programmed desorption of NH_3; L, Lewis acid sites; B, Brönsted acid sites.

(MTG), methanol to olefins (MTO), and methanol to propylene (MTP) have been attributed to the MTH reaction, which had been industrialized. Nonetheless, due to the low yield of BTX and rapid deactivation of catalysts by carbon deposition, the industrialization of methanol to aromatic (MTA) is limited [7–11].

Due to the presence of adjustable Brönsted acid sites, ion-exchange capacity, shape-selective character, and high hydrothermal stability, HZSM-5 has been widely used for MTA reaction [12–15]. However, the low catalytic effect of zeolite catalysts was attributed to intracrystalline diffusion limitations of catalysts, where the reagent and product diffusion to and from active sites was restricted. The introduction of mesopores into ZSM-5 zeolites was one of the most efficient strategies for enhancing the activity of the catalysts. Generally, mesopores were introduced into ZSM-5 zeolites by alkali treatment, thus increasing the diffusion rate of the products and the accessibility of reactants to active sites [16–18]. Additionally, HZSM-5 with mesoporous SiO_2 overlayer of several nanometer thickness was synthesized for reducing the effective diffusion length in zeolite channel and increasing the selectivity of *p*-xylene [19, 20]. The third strategy was desilication, nevertheless, due to the influence of Si/Al ratio and crystal size, the formation of evenly distributed and continuously ordered mesoporous by desilication was significantly challenging. Decilication solved the diffusion problem, increased the specific surface area, and caused additional acid sites to the catalyst [21–25]. As such, the removal of framework or amorphous silicon was the simplest and the most effective method in the formation of mesoporosity in HZSM-5 zeolites. Nonetheless, the active center of the MTA reaction hinged on the acid sites located in the pore, interpore, and surface of HZSM-5 zeolite. However, they were also the active centers of coke deposition, the intermediates of hydrocarbon or carbocation production during the reaction of MTA, which could be easily adsorbed onto these acid sites causing further growth without any restrictions. As a result, the acid sites were covered, a major reason for catalyst deactivation and low product selectivity [26, 27]. Moreover, due to the presence of stronger acidic site on the catalyst external surface, the secondary reactions (such as xylene isomerization) were generated resulting in by-products of heavy aromatics (denoted as C_{9+}) including ethylbenzene, trimethylbenzene, tetramethylbenzene, and high carbon paraffin in the MTA reaction [28–31]. In resolving these issues, the discovery of novel methods for enhancing the conversion of methanol and high selectivity of *p*-xylene remains significantly attractive but challenging.

Here, ammonium fluoride-treated and silane treated catalyst were synthesized. Then, the acid sites content and pore structure of Si/HZSM-5-0.09M were analyzed by NH_3-TPD. Moreover, N_2 adsorption–desorption and their activity was evaluated in methanol aromatization reaction. As a consequence, Si/HZSM-5-0.09M catalyst demonstrated an excellent activity and high *p*-xylene selectivity in methanol aromatization reaction.

EXPERIMENTAL

Catalyst Preparation

NH_4-ZSM-5 zeolite (Si/Al = 70) were purchased from Nanjing XFNANO Materials Tech Co., Ltd. (China). First, zeolite was calcined at 550°C for 6 h to remove the residual template. Then, HZSM-5 was treated using a NH_4F solution of different concentrations (0.07, 0.09, and 0.11 mol/L) to remove the framework Si. Typically, 10.0 g HZSM-5 zeolite was mixed with 200 mL NH_4F solution, stirred at 25°C for 10 h, washed, filtered, then dried at 110°C for 8 h, and calcined at 550°C for 6 h at a ramping rate of 5°C/min. The samples were denoted as HZSM-5-*x*M (x = 0.07, 0.09, and 0.11 mol/L).

The preparation of Si/HZSM-5-0.09M catalyst was as follows. Exactly 2.0 g HZSM-5-0.09M was added to the mixture consisting of 4.09 g tetraethoxysilane (TEOS) and 30 mL *n*-hexane under a reflux for 10 h at 75°C, stirring constantly. The solid product was recycled by filtration, washing, and drying overnight at 100°C and calcined at 550°C for 6 h. The silylated sample was synthesized and marked as Si/HZSM-5-0.09M. For comparison, the parent catalyst was similarly treated as above and denoted as Si/HZSM-5.

Catalyst Characterizations

The samples were characterized via X-ray diffraction (XRD) on a Rigaku D/Max-2400 (λ = 0.154 Å) with CuK_α radiation source operated at 40 kV and 150 mA. Scanning electron microscopic (SEM) images were generated from a JEOL 6701F instruments. The specific surface area and pore size distribution of the catalyst was determined via N_2 adsorption using a Quantachrome Autosorb-1 apparatus. Before testing, the catalyst was degassed by N_2 at 200°C for 3 h. The pore volume was determined at a relative pressure (P/P_0) of 0.99. The micropore area and volume were confirmed by the *t*-plot method, using the adsorption data range of $0.2 < P/P_0 < 0.6$. The NH_3-TPD was measured by a Autosorb-iQ-C chemisorptions, Quantachrome, USA. The XRF test was obtained on a Magic PW 2403 X while the Py-IR spectroscopy was performed on a Thermo Scientific (Nicolet 380).

Catalytic Activity Test

All evaluation experiments were conducted in a continuous fixed bed reactor made of stainless steel 700 mm long and 10 mm in inner diameter. The pro-

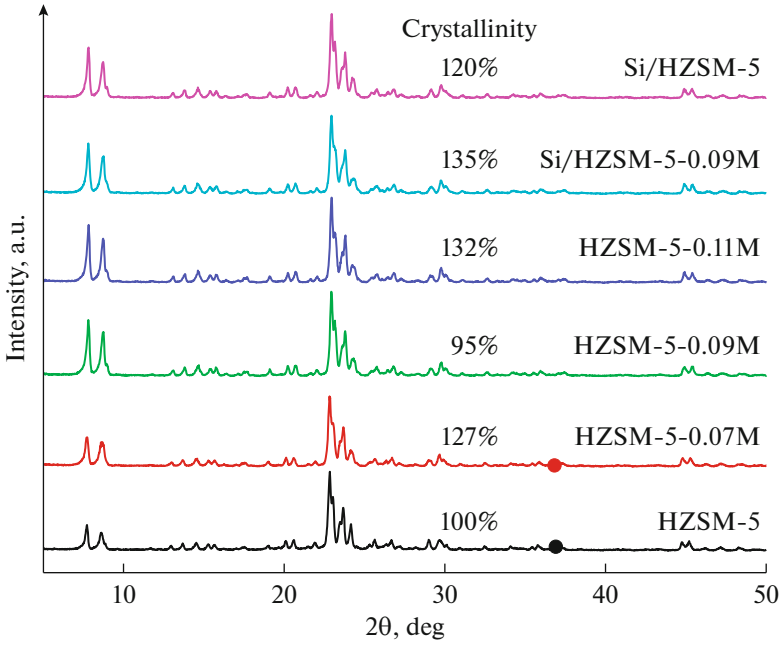

Fig. 1. XRD patterns of different catalysts.

cedure was as follows: 0.5 g of catalyst diluted with a quartz sand (5 g) was loaded in the middle of the tube reactor, then pretreated under 400°C in a N_2 flow (20 mL/min) for 1 h. Before adding to the reactor, methanol was firstly evaporized in the gasification chamber and then mixed with N_2 in the reactor. Products were analyzed using online gas chromatographs (Tianmei GC-7890II, Shanghai), which were equipped with flame ionization detectors (FID). SE-30 capillary columns were connected to FID.

Selectivity (S, wt %) and product yield (Y, wt %) were calculated by the formulas:

$$S_i = A_i n_i \Big/ \left(\sum A_i n_i\right) \times 100\%,$$
$$Y_i = X_{CH_3OH} S_i \times 100\%,$$

where X_{CH_3OH} is the conversion of CH_3OH; A is the peak area of the corresponding product on the gas chromatogram and n is the number of carbon atoms of the product i.

RESULTS AND DISCUSSION

Catalyst Characterizations

Figure 1 shows the XRD patterns of all samples in the 2θ range of 5°–50°. All of the samples exhibited the typical MFI topology whether processed via ammonium fluoride or silane treatment. An increase in the intensity of the diffraction peak at 2θ ~ 30° suggested that the relative crystallinity of catalysts was enhanced by ammonium fluoride treatment, further confirming the removal of silicate oligomers or amorphous silicon from HZSM-5 crystal [32]. The relative crystallinities of all the samples including Si/HZSM-5, HZSM-5-0.07M, HZSM-5-0.09M, HZSM-5-0.11M, Si/HZSM-5-0.09M were 127.0, 95.0, 132.0, 135.0 and 120.0% compared to HZSM-5 sample, respectively. Calculation method of relative crystallinity according to reference (see [33]). Surprisingly, Si/HZSM-5 demonstrated a higher crystallinity, which might be attributed to the formation of hydrogen bonds between the silicon hydroxyl group from TEOS dehydration synthesis and the hydroxyl group on the surface of the zeolite in the process of silanization. The contents of Al and F in the samples treated with ammonium fluoride were established by XRF technology (Table 1). No F was detected in all of the treated samples, probably because fluorine substituted oxygen or hydroxyl and bonded to silicon in the zeolite to form SiF_4, which was eventually removed in the roasting process. Moreover, no significant change was observed in the Al content of the samples treated with different fluoride concentrations suggesting that desilication was the main process upon zeolite fluorination treatment.

Figure 2a describes the N_2 adsorption/desorption isotherms and the corresponding pore-diameter distributions for the different catalysts. In the pressure range of $0 < P/P_0 < 0.5$, the adsorption isotherm curves of all catalysts displayed a sharp uptake indicated that all catalyst samples had typical micropore structure. This was consistent with the pore diameter distribution of the sample in Fig. 2b, and the microporous diameter of HZSM-5 was mainly concentrated between 1.2–1.8 nm. In the pressure range of $0.5 < P/P_0 < 0.95$, the isotherms of HZSM-5-0.09M and

Table 1. Al and F content in different samples

Samples	XRF content, wt %	
	Al	F
HZSM-5-0.07M	1.44	0
HZSM-5-0.09M	1.36	0
HZSM-5-0.11M	1.33	0
Si/HZSM-5-0.09M	0.857	0

Si/HZSM-5-0.09M attributed to the type IV isotherm with a hysteresis loop which might be due to the formation of secondary mesoporous structure by desilication, the mesoporous size was mainly about 2.5 nm. Furthermore, Fig. 2b reveals that many new micropores were generated after fluoride treatment. The large N_2 adsorbance of all samples was at $P/P_0 > 0.95$ attributed to the open mesopores connected to the external surface [34–36].

The textural properties (BET surface area (S_{BET}), micropore surface area (S_{micro}), mesopore surface area (S_{meso}), total pore volume (V_{total})) are summarized in Table 2. As seen from this table, the specific surface area and mesopore volume of HZSM-5-0.09M treated with an ammonium fluoride solution were higher than those of the original HZSM-5. At the same time, the specific surface area and volume of micropores of HZSM-5-0.09M were less than those of the original HZSM-5. This means that the removal of silicon transforms micropores into mesopores [37–39]. Subsequent silylation of HZSM-5 and HZSM-5-0.09M led to a further decrease in the specific surface area (Table 2). However, the pore volume of the Si/HZSM-5-0.09M catalyst remained almost unchanged, while the pore volume of the Si/HZSM-5 sample was significantly reduced. This is probably due to the TEOS passivation at the surface, which causes narrowing or blocking of the zeolite channels.

The morphology and crystal size of all samples are shown in Fig. 3. An HZSM-5 sample about 500 nm in size was made of crystals of about 30 nm (Fig. 3a). The amount of non-crystalline fine particles or aggregates of the zeolite was significantly reduced as a result of the zeolite treatment with an ammonium fluoride solution, as a result of the reaction with fluorine ions to form fluoride, which was further removed during calcination. This could be the reason for the increase in the intensity of the X-ray diffraction peak for the HZSM-5-0.09M sample (see Fig. 1). Nonetheless, after treatment with ammonium fluoride, the change of crystal morphology was not apparent (Fig. 3c), and this was associated with the special morphology of HZSM-5 zeolite and treatment conditions. The surface structures of Si/HZSM-5 and Si/HZSM-5-0.09M were tidier and less defective (Figs. 3b and 3d), suggesting their high crystallinity and stability [40].

Acid strength and concentration of all catalysts are shown in Fig. 4. There were 2 characteristic peaks (at 370 and 180°C) in the TPD-profiles which were assigned to the strong and weak acid sites, respectively. The change in the strength of the strong acid sites of the catalyst upon treatment with ammonium fluoride was not great and that of the weak acid sites was more noticeable. It should be noted that the order of decreasing intensity of the desorption peaks was as follows: HZSM-5-0.11M > HZSM-5-0.09M > HZSM-5-0.07M > HZSM-5. This was mainly due to the selective desilication by ammonium fluoride that induced the variation of coordination state Al, which triggered the variation of acid amount and/or acid strength. Xu et al. [32] confirmed that the treatment of zeolite with ammonium fluoride solution cuased selective desilication rather than dealumination, and the change of Al content was not associated with the increase of ammonium fluoride concentration. After silanization, the peak intensities of weak and strong acid sites decreased. Si/HZSM-5-0.09M had the lowest peak intensity of the strong sites. The strong and weak acid content of all samples is shown in Table 2. The content of strong and weak acid was significantly reduced by silanization, further confirming the effective passivation of external acid sites on Si/HZSM-5-0.09M.

Figure 5 demonstrates the IR spectra of pyridine adsorption on all samples. The IR band at 1453 and 1544 cm^{-1} belonged to L acid sites and B acid sites, respectively. Table 3 lists the test result of IR spectra of pyridine adsorption for all samples. We observed that

Table 2. Textural properties of all samples

Samples	S_{BET}[a], m^2/g	S_{micro}[b], m^2/g	S_{meso}[c], m^2/g	V_{total}[d], cm^3/g	V_{micro}[b], cm^3/g	V_{meso}[e], cm^3/g	Acid sites, mmol/g		
							total acid	weak acid	strong acid
HZSM-5	384	259	125	0.222	0.111	0.111	0.232	0.129	0.103
Si/HZSM-5	366	232	134	0.200	0.106	0.094	0.240	0.138	0.102
HZSM-5-0.09M	417	228	189	0.258	0.109	0.149	0.354	0.193	0.161
Si/HZSM-5-0.09M	391	244	147	0.240	0.110	0.130	0.251	0.152	0.099

[a] BET method. [b] *t*-Plot method. [c] $S_{meso} = S_{BET} - S_{micro}$. [d] Volume adsorbed at $P/P_0 = 0.99$. [e] $V_{meso} = V_{total} - V_{micro}$.

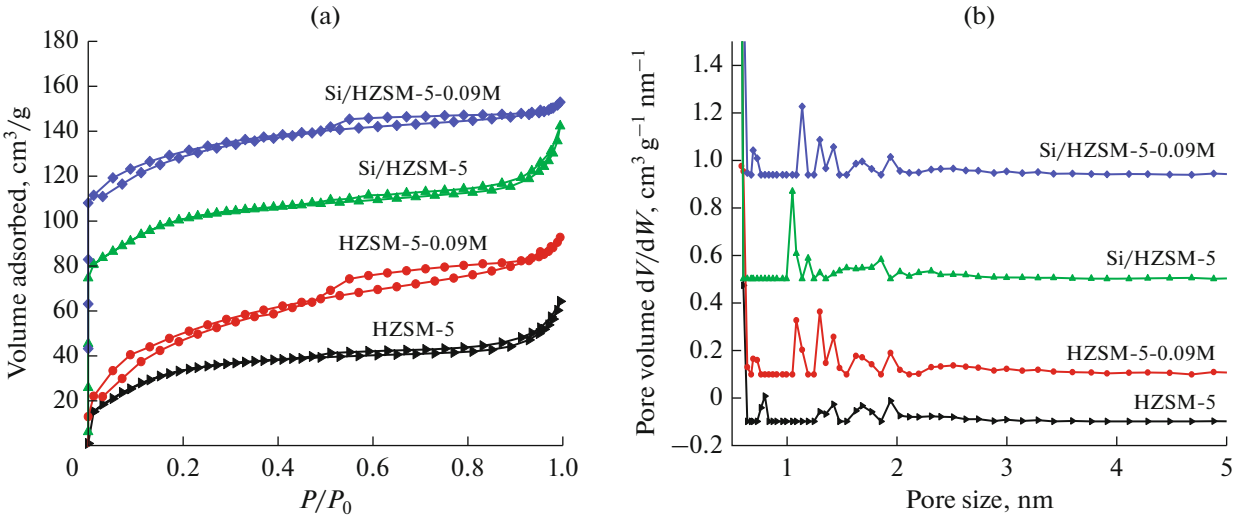

Fig. 2. N_2 adsorption/desorption isotherms and pore size distribution.

the amount of B acid sites and L acid decreased with increasing adsorption temperature. Besides, the total amount of B acid sites increased by the fluoride treatment while the L acid sites were decreased, this might be attributed to the selective removal of skeletal silicon from the zeolite resulting in fluorination, hence exposing more active aluminum centers. Although XRF characterization results revealed a slight reduction in Al content after fluorination, this effect was negligible. After silanization, the total amount of B acid sites decreased while that of the L acid sites increased, indicating that post-treatment regulated

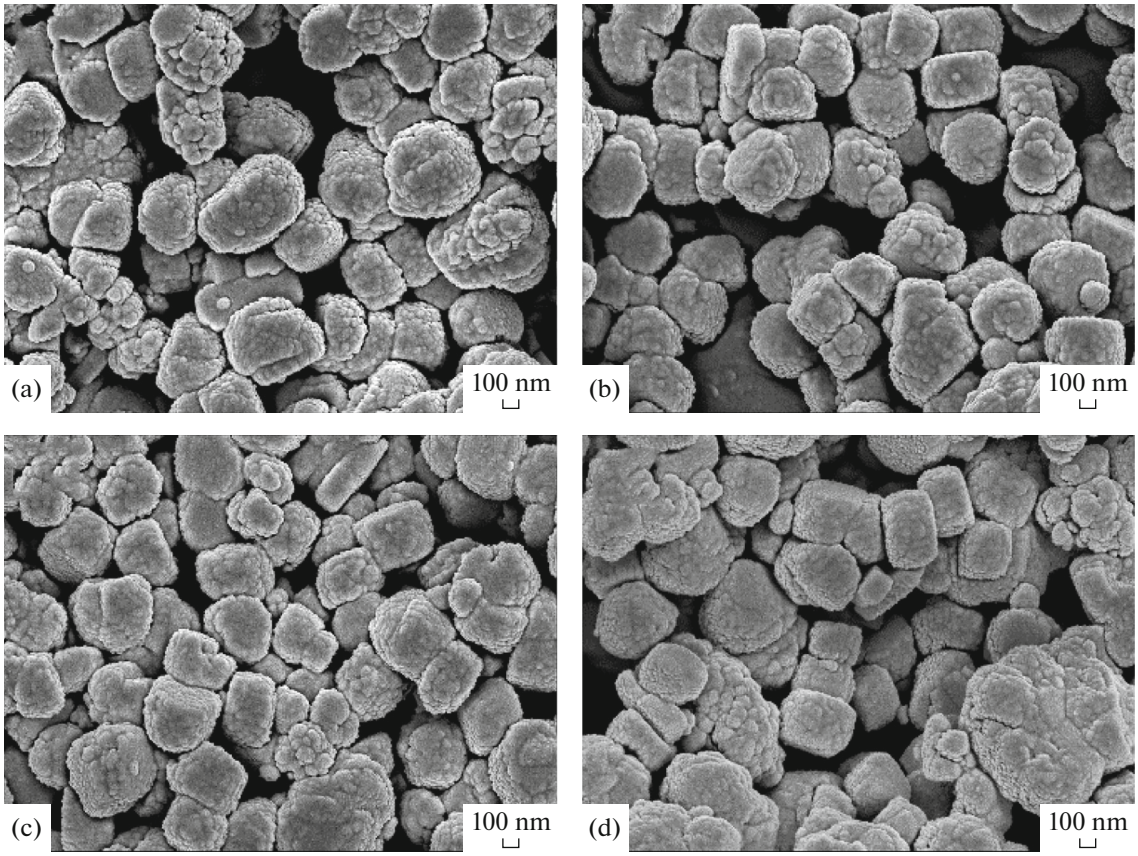

Fig. 3. Electron microscopy images of HZSM-5 (a), Si/HZSM-5 (b), HZSM-5-0.09M (c), Si/HZSM-5-0.09M (d).

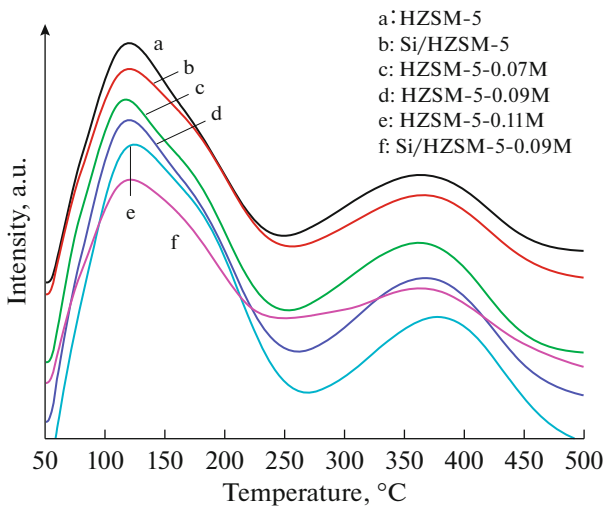

Fig. 4. NH_3-TPD profiles.

the distribution and concentration of acidic sites on the catalyst.

Catalytic Activity

The activity of all catalysts was evaluated in the MTA reaction. Table 4 shows the selectivity of products on different catalysts at TOS = 3 h. The selectivity of BTX over HZSM-5, Si/HZSM-5, HZSM-5-0.07M, HZSM-5-0.09M, HZSM-5-0.11M and Si/HZSM-5-0.09M catalysts were 33.0, 33.1, 44.6, 45.3, 43.1 and 54.8%, respectively. The selectivity of BTX was lowest over the HZSM-5 catalyst. Although the selectivity of aromatics on HZSM-5 and Si/HZSM-5 was insignificant, the *p*-xylene selectivity in isomers on HZSM-5 and Si/HZSM-5 was significantly different (39.0 and 65.0%, respectively). The HZSM-5-0.07M, HZSM-5-0.09M and HZSM-5-0.11M catalysts showed the highest BTX selectivity, which was primarily because of the higher density of acid sites and the removal of amorphous or framework silicon that provided many active sites for producing BTX.

Notably, the MTA reaction resulted in many products, and continuous isomerization reaction on the outer surface of the catalysts thereby generated additional complex products. The separation and purification of the later products containing xylene isomers were more difficult due to the presence of isomers. In the MTA reaction, if the formation of by-products was inhibited, the single conversion of raw materials into high value-added aromatic products (such as *p*-xylene) saved the cost in the later stage and exhibited an important significance for the industrialization process of MTA reaction. Therefore, we comprehensively analyzed the composition of products on 6 catalysts. Fig. 6a shows the distribution of hydrocarbons in the MTA reaction. The highest selectivity of BTX was found over Si/HZSM-5-0.09M catalyst, which was majorly because of the higher xylene selectivity, specifically *p*-xylene. Additionally, the selectivity of C_{9+} over HZSM-5-0.07M and Si/HZSM-5-0.09M was significantly reduced, suggesting that the mesopores generated by desilication effectively reduced the diffusion resistance of the products with large molecular dynamics diameters. Fig. 6b demonstrates the *p*-xylene and BTX selectivity over different catalysts. The *p*-xylene selectivity over HZSM-5, Si/HZSM-5, HZSM-5-0.07M, HZSM-5-0.09M, HZSM-5-0.11M and Si/HZSM-5-0.09M catalyst were 4.6, 7.2, 9.0, 13.8, 12.2 and 19.8%, respectively. Among HZSM-5-0.07M, HZSM-5-0.09M, and HZSM-5-0.11M catalysts, HZSM-5-0.09M demonstrated the highest BTX selectivity. This was primarily due to partial coverage

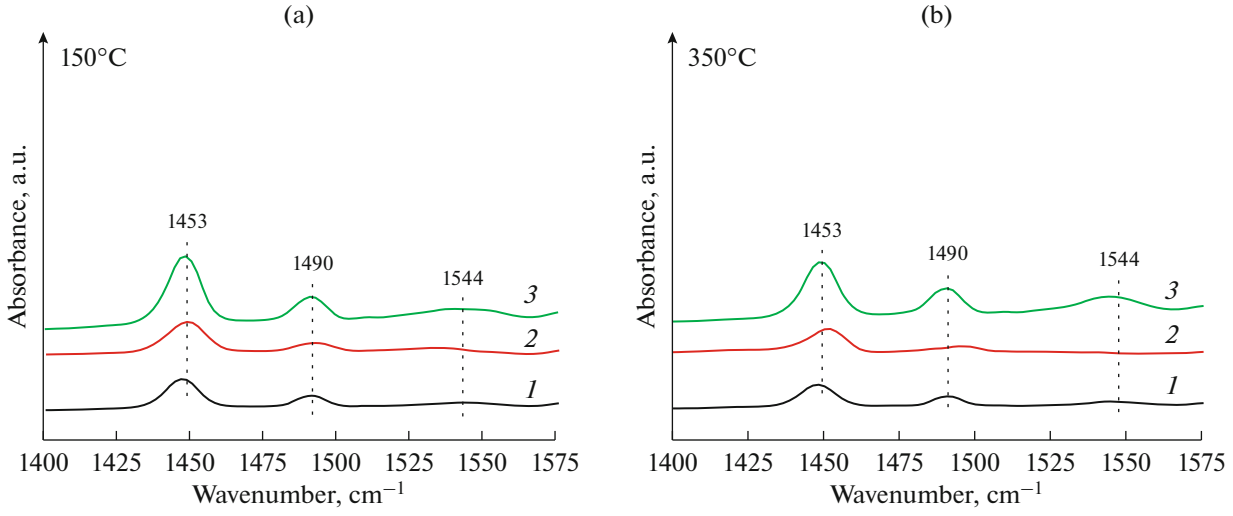

Fig. 5. IR spectra of pyridine adsorbed on HZSM-5 (*1*), HZSM-5-0.09M (*2*) and Si/HZSM-5-0.09M (*3*) at 150 (a) and 350°C (b).

Table 3. Catalyst acidity derived from IR spectra of adsorbed pyridine

Catalysts	Amount of B, mg/cm^2			Amount of L, mg/cm^2			B/L
	150°C	350°C	total	150°C	350°C	total	
HZSM-5	3.47	3.47	6.94	77.6	46.8	124.4	0.05
HZSM-5-0.09M	13.1	0.54	13.6	51.7	24.4	76.1	0.17
Si/HZSM-5-0.09M	5.19	3.36	8.55	113	62.3	175	0.04

Table 4. Product distribution over different catalysts

Catalysts	Selectivity, wt %									Selectivity$_{BTX}$, wt %
	C_1	C_2	C_3	C_4	C_{5+}	B	T	X	C_{9+}	
HZSM-5	2.9	7.3	11.2	14.2	11.6	19.1	2.3	11.6	19.8	33
Si/HZSM-5	2.8	6.8	8.0	9.6	16.6	15.5	6.6	11.0	23.1	33.1
HZSM-5-0.07M	1.6	6.4	6.9	10.8	24.9	15.5	17.1	12.0	4.6	44.6
HZSM-5-0.09M	1.0	4.1	5.3	5.4	20.8	12.6	13.1	19.6	18.1	45.3
HZSM-5-0.11M	1.8	6.0	7.1	8.6	14.7	14.8	11.1	17.2	18.7	43.1
Si/HZSM-5-0.09M	1.2	4.8	7.9	8.6	15.3	16.2	7.9	30.7	7.4	54.8

of the acid sites on the outer surface after silanization. As a result, the isomerization reaction was inhibited and the *p*-xylene selectivity was significantly improved. In the case of complete conversion of methanol, although the selectivity of the target product could be improved, the stability of catalyst activity remains a significant challenge in the MTA reaction.

In this work, MTA reactions were performed at low pressure, low temperature, and low airspeed. Each catalyst for the MTA reaction required precise reaction conditions. Therefore, to obtain a maximum product selectivity, it is essential to evaluate reaction conditions including temperature and airspeed. Figure 7 shows influence of reaction conditions in MTA reaction over Si/HZSM-5-0.09M on the selectivity. As seen in Fig. 7c, the selectivity of C_1 increased with the increasing of temperature from 350 to 500°C, but $C_2^=$–$C_4^=$ remained almost unchanged with the increase of temperature, while C_{5+} decreased with the increase of temperature. Note that the selectivity of BTX was

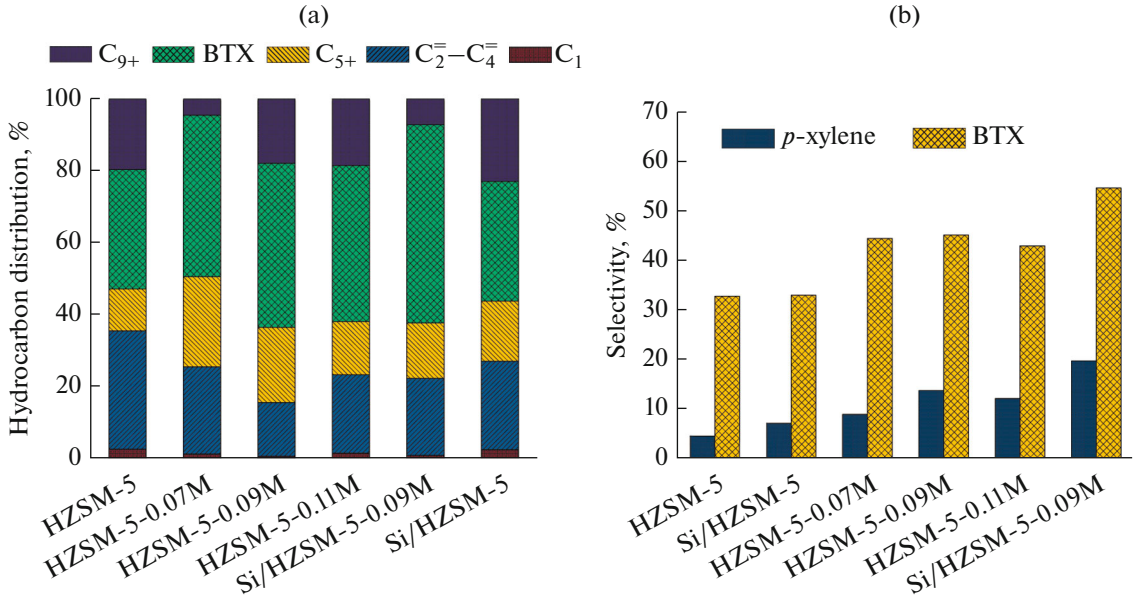

Fig. 6. Distribution of hydrocarbons in the MTA reaction (a) and selectivity of *p*-xylene and BTX (b) on different catalysts.

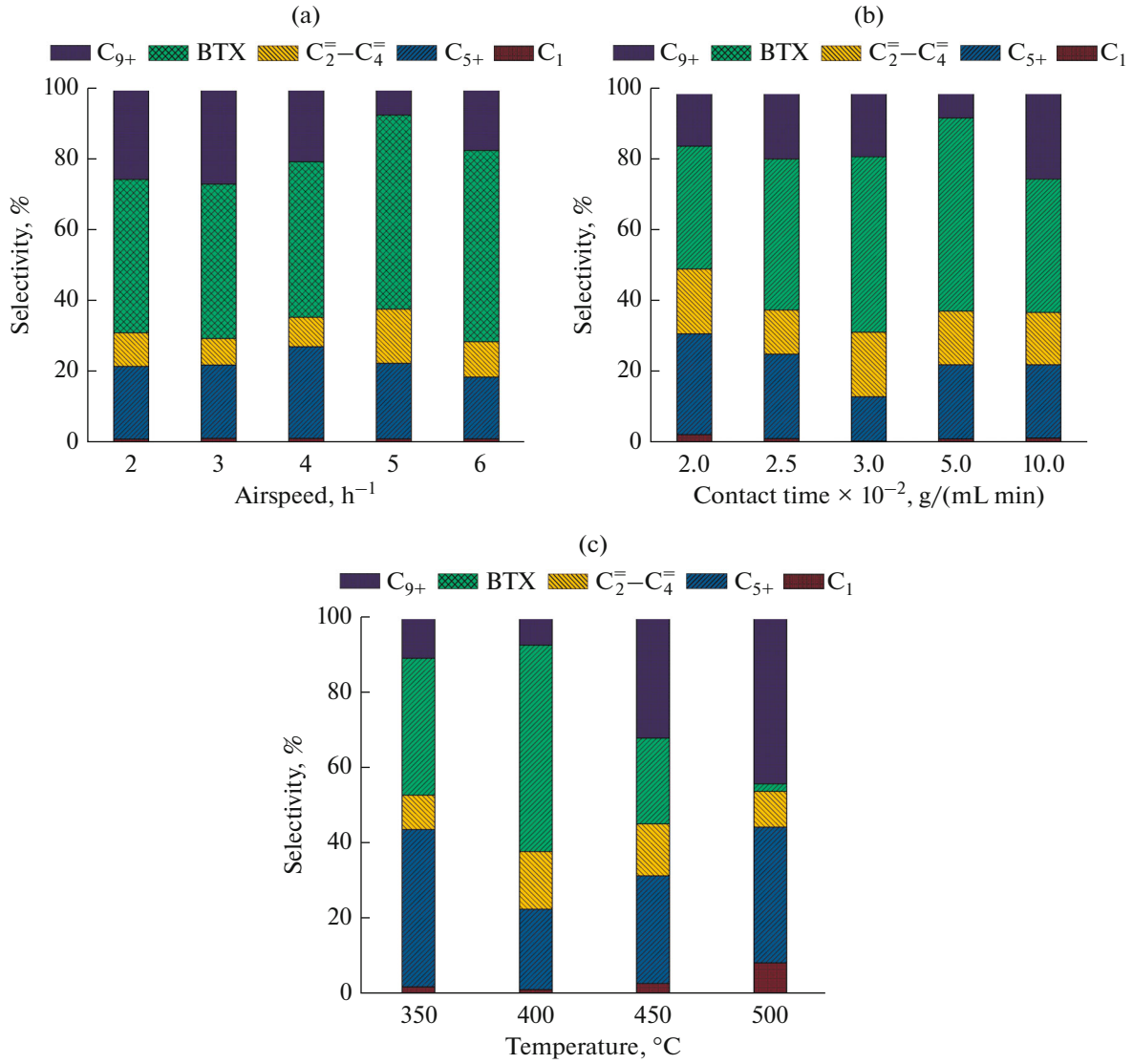

Fig. 7. Effect of reaction conditions for the catalytic performance of Si/HZSM-5-0.09M. (a) Effect of airspeed. Reaction conditions: 0.1 MPa, 400°C, 0.02 g/(mL min), m_{cat} = 0.5 g. (b) Effect of contact time. Reaction conditions: 0.1 MPa, 400°C, 5 h^{-1}, m_{cat} = 0.5 g. (c) Effect of temperature. Reaction conditions: 0.1 MPa, 5 h^{-1}, 0.05 g/(mL min), m_{cat} = 0.5 g.

the highest at 400°C. With increasing temperature, the selectivity of BTX sharply dropped, while the selectivity of C_{9+} increased. The main reason was, first of all, that the water produced in the reaction process caused the loss of framework Al of the catalyst under the condition of high temperature, the collapse of the framework of catalyst, and[REMOVED HYPERLINK FIELD] irreversible inactivation. Also, airspeed and contact time were important factors influencing the product distribution of the MTA reaction. As shown in Figs. 7a and 7b, the productivity of BTX increased with the increase of airspeed and contact time then declined when airspeed and contact time decreased continuously, notably, this was primarily attributed to the less secondary reactions. Additionally, the single treatment capacity of the catalyst was limited, indicating that if the contact time was too long, the product would gradually spread, finally causing carbon deposition. Therefore, reducing airspeed or shortening the contact time to eliminate the diffusion limitation was also a vital factor, thereby influencing the activity of the catalyst for guaranteeing the highest yield of the product.

Figure 8 shows the change trend of selectivity over Si/HZSM-5-0.09M and HZSM-5 catalysts within 12 h. Si/HZSM-5-0.09M revealed a higher BTX selectivity in 12 h and a longer catalyst life than HZSM-5. The main reason was that Si/HZSM-5-0.09M had a larger specific surface area and pore volume exposed to more acid sites as the active center of MTA reaction known from the analysis of BET and NH_3-TPD. On the other hand, N_2 adsorption/desorp-

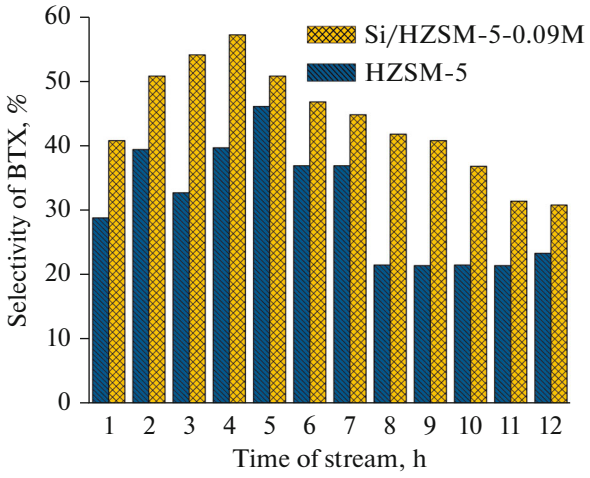

Fig. 8. BTX selectivity on HZSM-5 and Si/HZSM-5-0.09M vs. time on stream.

tion isotherms (Fig. 2) demonstrated that Si/HZSM-5-0.09M had apparent micro/mesoporous structure and special hierarchical pore structure. This characteristic was beneficial to shape-selective catalysis, promoted the diffusion rate of reactant/product, and reduced the secondary reaction on catalyst surface [41]. Therefore, Si/HZSM-5-0.09M catalyst showed an effective methanol aromatization performance with a potential to realize industrialization of MTA reaction.

Based on catalyst characterization and evaluation results, ammonium fluoride treatment had a significant effect on the catalytic effect of HZSM-5 by MTA reaction. Appropriate ammonium fluoride concentration enhanced the selectivity of aromatics and improved the stability of catalysts. After the treatment of HZSM-5 by ammonium fluoride, the crystallinity of HZSM-5 improved due to amorphous silicon on the outer surface being dissolved. Therefore, more acidic sites exposed were more conducive to the conversion of methanol, namely the generation of aromatic hydrocarbons. However, beyond that, the channel structure of catalysts was a key factor for the selectivity of the target product. The reason was that an appropriate channel structure was conducive to the shape-selectivity of products, improved the mass transfer limit or weak internal diffusion limitation, and extended the lifetime of the catalysts. Regarding the diffusion path of aromatics in the channel of HZSM-5, it was confirmed that aromatics spread from the straight channel of HZSM-5, and olefins diffused in both straight and sinusoidal channels. The straight path was short, significantly reducing the isomerization of aromatic hydrocarbons in the channel [41]. After ammonium fluoride treatment, the specific surface area and pore volume of mesoporous HZSM-5 significantly increased. Mesoporous specific surface area increased from 111 to 175 m^2/g, mesoporous pore volume enhanced from 0.084 to 0.099 mmol/g, and the total acidity grew from 0.232 to 0.354 cm^3/g, leading to the total selectivity of aromatics from 33.0 to 45.3%. The above data reveal that HZSM-5 treated with ammonium fluoride was an effective post-treatment modification method, with a satisfactory industrial application prospect in the MTA reaction.

CONCLUSIONS

In conclusion, we prepared Si/HZSM-5-0.09M catalyst via desilication, then evaluated the re-growth of silicon and catalytic activity by the MTA reaction. The experimental results revealed that the total selectivity of aromatics on Si/HZSM-5-0.09M catalyst was up to 54.8%, particularly, the selectivity of *p*-xylene was up to 19.8% under the optimal reaction conditions. Furthermore, we discussed and compared the isomerization reactions on different catalysts. Si/HZSM-5-0.09M catalyst was found to demonstrate a satisfactory aromatization performance after removal of amorphous silicon and re-growth of crystal silicon. Primarily this was attributed to improvement of the catalyst microstructure (crystal size, pore channel, specific surface area) and to the adjustment of acidity of HZSM-5 zeolite because of a suitable reaction environment for the MTA reaction. Thus, Si/HZSM-5-0.09M catalyst demonstrated the potential of industrialization for the MTA reaction.

FUNDING

We acknowledge financial support from the National Natural Science Foundation of China (no. 21666019) and the science and technology support project of Gansu province (1604GKCD026).

CONFLICT OF INTEREST

The authors declare that they have no conflicts of interest.

REFERENCES

1. Olah, G.A., Goeppert, A., and Prakash, G.S., *J. Org. Chem.,* 2009, vol. 74, p. 487.
2. Zhao, Y., Tan, W., and Wu, H., *Catal. Today*, 2011, vol. 60, p. 179.
3. Jiang, G.Y., Zhang, L., and Zhao, Z., *Appl. Catal., A*, 2008, vol. 340, p. 176.
4. Wang, C.F., Zhang, Q., and Zhu, Y.F., *Mol. Catal.*, 2017, vol. 433, p. 242.
5. Weber, J.L., Dugulan, I., and Jongh, P.E.D., *ChemCatChem,* 2017, vol. 10, p. 1107.
6. Jia, L.Y., Raad, M., and Hamieh, S., *Green. Chem.*, 2017, vol. 19, p. 5442.
7. Cui, Z.M., Liu, Q., and Song, W.G., *Angew. Chem. Int. Ed.*, 2006, vol. 118, p. 6662.
8. Konnov, S.V., Pavlov, V.S., Ivanova, II., and Khadzhiev, S.N., *Petrol. Chem.*, 2016, vol. 56, p. 1154.

9. Haw, J.F., Song, W., Marcus, D.M., and Nicholas, J.B., *Acc. Chem. Res*., 2003, vol. 36, p. 317.
10. Unni, O., Stian, S., Morten, B., Pablo, B., Finn, J., and Silvia, B., *Angew. Chem, Int. Ed*., 2012, vol. 51, p. 5810.
11. Schulz, H., *Catal. Today*, 2010, vol. 154, p. 183.
12. Li, W.L., Li, F., Wang, H.Y., Liao, M.J., Li, P., Zheng, J.J., and Tu, C.Y., *Mol. Catal*., 2020, vol. 480, p. 1.
13. Wang, X.N., Zhang, J.F., and Zhang, T., *RSC. Adv*., 2016, vol. 6, p. 23428.
14. Ghavipour, M., Behbahani, R.M., and Moradi, G.R., *Fuel*, 2013, vol. 113, p. 310.
15. Zhang, G., Xin, Z., and Bai, T., *J. Energy Chem*., 2015, vol. 24, p. 108.
16. Tian, H., Lv, J., Liang, X., and Zha, F., *Energy Technol.-Ger*., 2018, vol. 119, p. 1.
17. Sònia, A., Bonilla A. Pérez-Ramírez, J, *Appl. Catal., A,* 2009, vol. 364, p. 191.
18. Mochizuki, H., Yokoi, T., and Imai, H., *Appl. Catal., A*, 2012, vol. 449, p. 188.
19. Lu, P., Fei, Z.Y., and Li, L., *Appl. Catal., A*, 2013, vol. 453, p. 302.
20. Dong, P., Li, Z.Y., and Wang, D.L., *Catal. Lett*., 2018, vol. 149, p. 248.
21. Groen, J.C., Bach, T., and Ziese, U., *J. Am. Chem. Soc.,* 2005, vol. 127, p. 10792.
22. Unni, O., Stian, S., Morten, B., Pablo, B., Finn, J., and Silvia, B., *Angew. Chem., Int. Ed*., 2012, vol. 51, p. 5810.
23. Schulz, H., and Wei, M., *Top. Catal.,* 2014, vol. 57, p. 683.
24. Liu, Z., Dong, X., and Liu, X., *Catal. Sci. Technol*., 2016, vol. 6, p. 8157.
25. Xin, H., Li, X., and Fang, Y., *J. Catal.* 2014, vol. 312, p. 204.
26. Mores, D., Kornatowski, J., and Olsbye, U., *J. Chem. Eur*., 2011, vol. 17, p. 2874.
27. Rownaghi, A.A., Rezaei, F., and Hedlund, J., *Microporous Mesoporous Mater*., 2012, vol. 151, p. 26.
28. Li, N., Meng, C., and Liu, D.H., *Fuel*, 2018, vol. 233, p. 283.
29. Gao, P., Xu, J., Qi, G.D., Wang, C.Q., and Zheng, Y.X., *ACS Catal*., 2018, vol. 8, p. 9809.
30. Dai, Q.G., Bai, S.X., Wang, X.Y., and Lu, G.Z., *J. Porous. Mater*., 2014, vol. 21, p. 1041.
31. Liu, F.J., Willhammar, T., and Wang, L., *J. Am. Chem. Soc*., 2012, vol. 134, p. 4557.
32. Xu, T., Zhang, Q., and Song, H., *J. Catal*., 2012, vol. 295, p. 232.
33. Wang, N., Hou, Y., Sun, W., Cai, D., Chen, Z., and Liu, L., *Appl. Catal., B*, 2019, vol. 243, p. 721.
34. Sugi, Y., Kubota, Y., and Komura, K., *Appl. Catal., A*, 2006, vol. 299, p. 157.
35. Xin, H.C., Li, X.P., and Li, X.P., *J. Catal*., 2014, vol. 312, p. 204.
36. Groen, J.C., Peffer, L.A.A., and Pérez-Ramírez, J., *Microporous Mesoporous Mater*., 2003, vol. 60, p. 1.
37. Kwok, K.M., Ong, S.W.D., Chen, L.W., and Zeng, H.C., *ACS Appl*., 2019, vol. 11, p. 14774.
38. Hasan, Z., Jun, J.W., and Kim, C.U., *Mater. Res. Bull.,* 2015, vol. 61, p. 469.
39. Wan, W.L., Fu, T.J., Qi, R.Y., and Li, Z., *Ind. Eng. Chem. Res*., 2016, vol. 55, p. 13040.
40. Pérez-Ramírez, J., Christensen, C.H., and Egeblad, K., *Chem. Soc. Rev*., 2008, vol. 37, p. 2530.
41. Zhang, J.G., Qian, W.Z., Kong, C.H., and Wei, F., *ACS Catal*., 2015, vol. 5, p. 2982.